

# Coupling finite and boundary element methods to solve the Poisson-Boltzmann equation for electrostatics in molecular solvation

Author A<sup>\*</sup>, Author B<sup>†</sup>, Author C<sup>‡</sup> Author D<sup>§</sup>

March 4, 2022

## Abstract

Abstract

**Keywords:** Finite element method, Boundary element method, Poisson-Boltzmann, Implicit solvent model, Electrostatics. ■

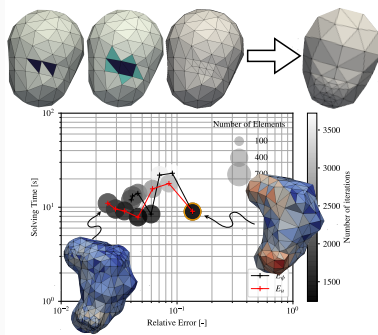
---

<sup>\*</sup>Department of Biology, University 1, ...

<sup>†</sup>Department of Chemistry, University 2, ...

<sup>‡</sup>Department of Physics, University 3, ...

<sup>§</sup>Department of Mathematics, University College London, ...



(75 words.) Images for the graphical Table of Contents should capture the essence of a paper, displaying a figure, plot, or scheme that is central to the theme of the manuscript. The text of the graphical Table of Contents is meant for the non-specialist and should ideally contain no obscure jargon or mathematical symbols / equations, but should attempt to convey the gist of the paper in everyday terms, while remaining consistent with accepted standards of scientific literature.

# INTRODUCTION

In biologically relevant settings, the structure and function of biomolecules is largely determined by the surrounding water with salt. To describe these systems accurately, we need to account for the solvent correctly, which has given rise to a wide range of models [cite water review] Highly detailed models consider every water molecule and salt ion explicitly, however, there are approximated models that use continuum theory to represent this ionic solution, known as implicit-solvent models [SimonsonRoux, DescherchiRocchia]. In the case of electrostatics, the implicit-solvent model is mathematically characterized by the Poisson-Boltzmann equation (PBE) [Baker,Bardhan], which is widely used to compute solvation free energies and mean-field potentials.

The implicit-solvent model for electrostatics describes the dissolved molecule as a infinite medium with a low-dielectric solute-shaped cavity, which contains a charge distribution from the partial charges (usually a sum of Dirac deltas at the atom’s locations). The outer solvent region is represented with a high dielectric, and considers the presence of salt. These two regions are interfaced by the molecular surface, which can be defined in various ways [cite], where the continuity of the electrostatic potential and electric displacement are enforced.

The PBE has been solved numerically with finite difference [cite], finite element [cite], boundary element [cite], and analytical [cite] methods. In particular, the boundary element method (BEM) has proven to be very efficient for high accuracy calculations [GengKrasny2013,CooperBardhan] mainly due to the precise description of the molecular surface and point charges. However, BEM is limited to constant material properties in each region, and the linear version of the PBE. Even though these limitations are acceptable in a wide range of applications, there are cases when BEM falls short, for example, if a variable permittivity is required inside the solute [cite], or the solute is highly charged such that the linear approximation breaks [cite?].

This article presents a methodology to overcome some of those limitations, through coupling boundary and finite elements (FEM-BEM). This approach brings the best of both worlds: the flexibility of FEM and efficiency of BEM, all in an accurate description of the dissolved molecule.

# METHODOLOGY

## The implicit solvent model

The implicit solvent model can be described mathematically as a coupled system of partial differential equations, where the Poisson-Boltzmann governs in the solvent region ( $\Omega_X$  in Figure XX), and the Poisson equation in the solute region ( $\Omega_Y$  in Figure XX). These regions are interfaced by the molecular surface ( $\Gamma$ ), where the potential ( $\phi$ ) and electric displacement ( $\epsilon \partial \phi / \partial \mathbf{n}$ ) are continuous.

$$\begin{aligned} \nabla^2 \phi_1(\mathbf{x}) &= \frac{1}{\epsilon} \sum_{k=1}^{N_q} q_k \delta(\mathbf{x}, \mathbf{x}_k) \quad \mathbf{x} \in \Omega_1 \\ (\nabla^2 - \kappa^2) \phi_2 &= 0 \quad \mathbf{x} \in \Omega_2 \\ \phi_1 &= \phi_2 \quad \epsilon_1 \frac{\partial \phi_1}{\partial \mathbf{n}} = \epsilon_2 \frac{\partial \phi_2}{\partial \mathbf{n}} \quad \mathbf{x} \in \Gamma. \end{aligned} \tag{1}$$

where  $\epsilon_1$  and  $\epsilon_2$  are the dielectric constants in the solute and solvent, respectively,  $\kappa$  is the inverse of the Debye length, related with the salt concentration, and  $q_k$  are the values of the partial charges, located at  $\mathbf{x}_k$ .

The electrostatic potential in  $\Omega_1$  can be further decomposed into singular and regular components as  $\phi_1 = \phi_c + \phi_R$ , where  $\phi_c$  is the solution to

$$\begin{aligned} \nabla^2 \phi_c(\mathbf{x}) &= \frac{1}{\epsilon_1} \sum_{k=1}^{N_q} q_k \delta(\mathbf{x}, \mathbf{x}_k) \quad \mathbf{x} \in \Omega_1 \cup \Omega_2 \\ \phi_c(\mathbf{x}) &= 0 \quad \text{as } |\mathbf{x}| \rightarrow \infty \end{aligned} \tag{2}$$

Physically,  $\phi_c$  can be interpreted as the Coulomb-type potential from the point charges, whereas  $\phi_R$ , also known as reaction potential, is originated by the polarization of the solvent. Usually,  $\epsilon_1$  is considered a constant value, yielding an analytical expression for  $\phi_c$ , however, this is not the general case.

There are regularized versions of Equation (1) [HolstETal2008,GengZhao2020] which are widely used to numerically solve the Poisson-Boltzmann equation with finite element or finite difference methods. However, here we use the standard formulation in Equation (1), as it offers more flexibility when dealing with, for example, variable permittivities.

A common quantity of interest in implicit solvent models is the solvation free energy, which the change in Gibbs free energy as the molecule moves from vacuum into the solvent. Considering the charge distribution  $\rho$  consists of point charges, this can be calculated as

$$\Delta G_{solv} = \frac{1}{2} \int_{\Omega_1} \rho(\mathbf{x}) \phi_r(\mathbf{x}) = \frac{1}{2} \sum_{k=1}^{N_q} q_k \phi_r(\mathbf{x}_k) \quad (3)$$

## Numerical solution of the Poisson-Boltzmann equation

### BEM-BEM coupling

- Direct formulation

### FEM-BEM coupling

- Description with constant and variable permittivity
- Standard BEM-BEM and FEM-BEM coupling approach
- Hybrid FEM-BEM coupling

## RESULTS

This section presents verification and performance results of the standard and hybrid FEM-BEM coupling schemes, for molecules modeled as cavities with constant and varying permittivity. When the permittivity inside the molecule was constant, we tested convergence against the available analytical expression of the solvation energy of a sphere [Kirkwood1934], and then compared a more realistic geometry (arginine) with a purely BEM implementation. On the other hand, we considered a Gaussian-varying permittivity [Alexov and earlier] inside arginine, and used APBS [Baker2001] to verify. The final result of this section shows the scaling of the standard and hybrid FEM-BEM coupling, as the molecule size grows.

All runs were done on XX computer with YY specifications.

## Results with constant permittivity

In implicit-solvent models, the molecule is usually considered as a region with constant permittivity, in this case, with  $\epsilon_1 = 4$ . In the solvent region, we used the permittivity of water ( $\epsilon_2=80$ ) and an inverse of the Debye length of  $\kappa = 0.125 \text{ \AA}^{-1}$ .

### Convergence of a spherical cavity

The Kirkwood sphere [Kirkwood1934] is a standard benchmark for the Poisson-Boltzmann equation in molecular electrostatics. Here, we considered a spherical cavity with radius  $R = 2 \text{ \AA}$ , with three charges ( $q_1=1$ ,  $q_2=1$ , and  $q_3=0.75$ ) placed at  $\mathbf{x}_1 = (1, 0, 0)$ ,  $\mathbf{x}_2 = (0.7, 0.7, 0)$ , and  $\mathbf{x}_3 = (-0.5, -0.5, 0)$ . Figure 1 shows the error convergence of the standard and hybrid FEM-BEM approaches, and a reference BEM implementation, to the analytical solution ( $\Delta G_{solv} = -164.33752347454015 \text{ kcal/mol}$ ). In these runs, the FEM mesh was generated using Bempp (check?) from a surface discretization with W, X, Y, and Z vertices per  $\text{\AA}^2$  on the SES, which was also used for the BEM runs. For the hybrid FEM-BEM coupling approach, we used  $\tau=10$ .

The error in Figure 1 decays linearly with the surface area, which agrees with the expected convergence for P1 elements, indicating a correct implementation of the numerical scheme. We can see that the purely BEM implementation outperforms (or not?) FEM-BEM coupling in terms of accuracy for equivalent meshes, and also that the hybrid approach does not (or does?) influence accuracy.

### Performance for arginine

As a more realistic test, we assessed the performance of the standard and hybrid FEM-BEM coupling techniques against a purely BEM implementation for arginine [cite arg]. We generated surface meshes containing W, X, Y, and Z vertices per  $\text{\AA}^2$  with Nanoshaper [Rocchia]. These meshes were inputs to our purely BEM solver, and to create the FEM mesh with pyGAMer [pygamer], invoking `tetgen` with the string `abcd`. For the hybrid FEM-BEM coupling approach, we used  $\tau=10$ .

Figure ?? compares the time-to-solution with the three schemes, and shows that using

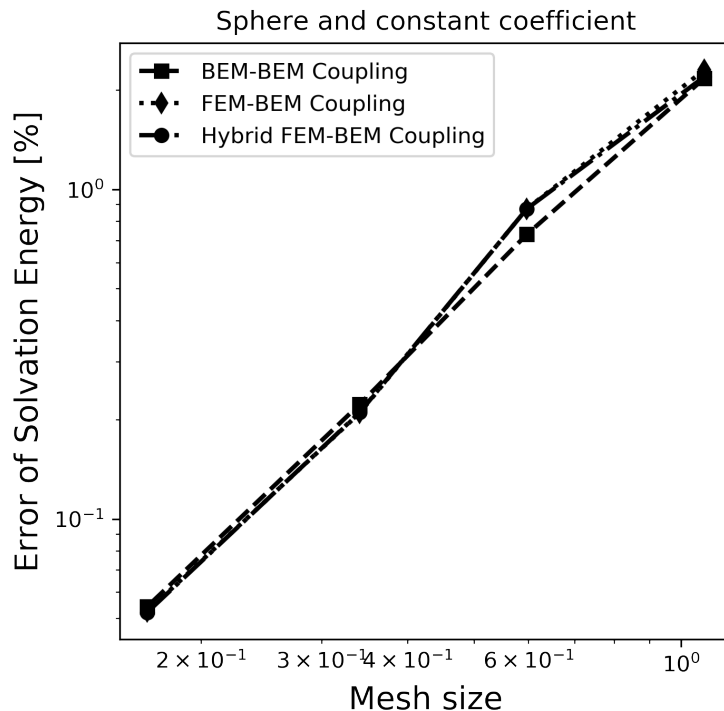


Figure 1: Error for the Kirkwood sphere.

only BEM outperforms both coupled FEM-BEM approaches. Even though hybrid FEM-BEM is slower than standard FEM-BEM in Figure ??, the iteration count in Figure ?? shows that hybrid FEM-BEM needs less iterations (can we compare them?). This behavior is promising going towards larger problems, specially since the hybrid approach allows for more flexibility in the choice of preconditioner. We can also see that accuracy is not affected (or is?) by considering a FEM region inside the molecule (need fig to check this).

Do we really need to compute the vacuum case numerically? We should be able to do it analytically, right?

## Results with variable permittivity

In contrast to a purely BEM approach, FEM-BEM coupling gives flexibility to consider space-varying field parameters. A popular description of the molecule is to consider a permittivity that varies like a Gaussian around each atom [earlier papers], which has shown enhanced accuracy in some applications, like binding energy calculations (check) [Alexov]. In this

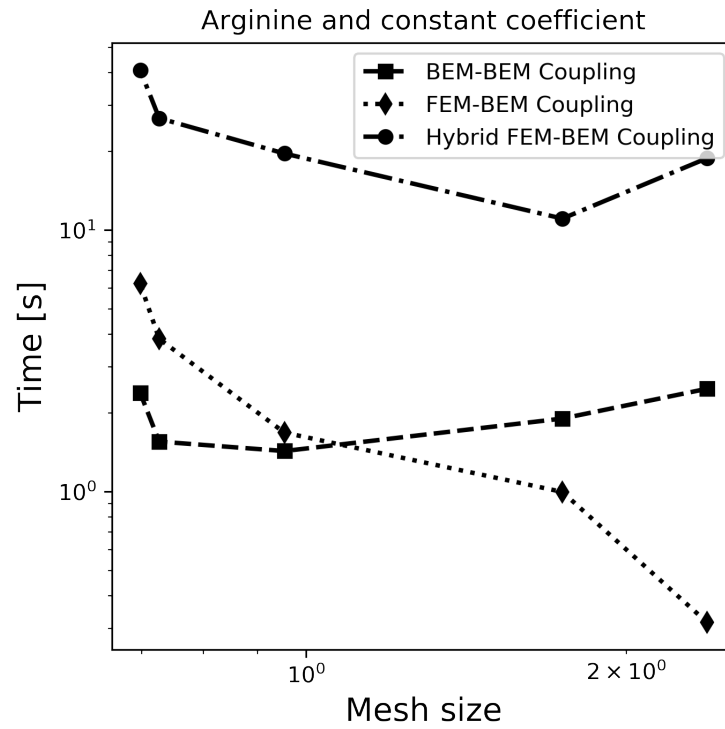


Figure 2: Time-to-solution for arginine with a constant permittivity. maybe we could also add a "error" wrt extrapolation, or a plot with energy for each mesh?



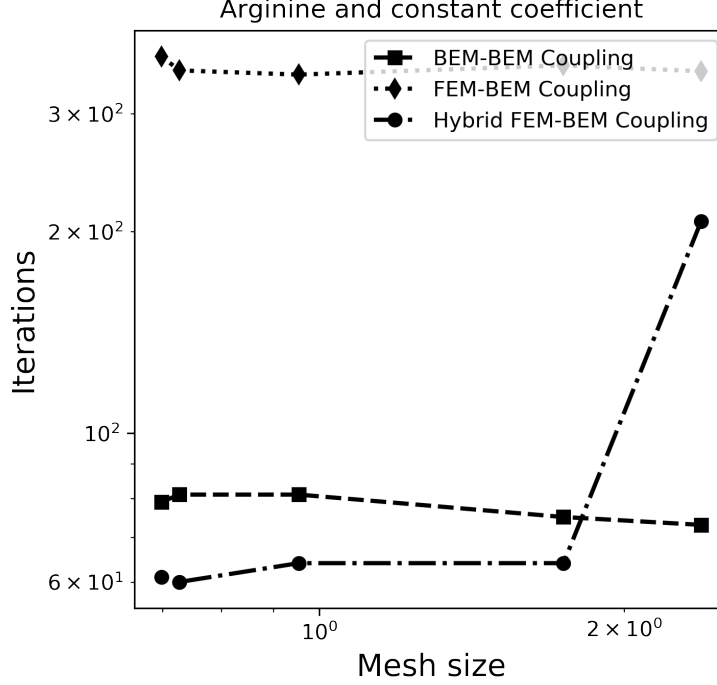


Figure 3: Iteration count for arginine with a constant permittivity.

setting, we define a density function  $\rho$  depending on position  $r$  as

$$\rho(r) := \prod_i \left( 1 - \exp \left( -\frac{\|r - \mathbf{x}_i\|}{\sigma^2 R_i^2} \right) \right) \quad (4)$$

where the product is over the atoms of the solute,  $R_i$  is the vdW radius of atom  $i$  and we used  $\sigma=1$ . Then, we can compute the permittivity as

$$\epsilon := (1 - \rho) \epsilon_1 + \rho \epsilon_2 \quad (5)$$

We used Equation (??) to generate dielectric maps, which we ran on APBS for comparison. As  $\epsilon_2$  is variable, Equation (??) does not have an analytical solution, and the electrostatic potential in vacuum state has to be computed numerically. For vacuum calculations, we considered the same distribution of  $\epsilon$  inside the molecule as in the solvated case, however, the solvent permittivity was set to  $\epsilon=2$ . Other implementations of Gaussian permittivities also modify the solute permittivity in vacuum calculations, according to a set cutoff [Alexov]. We did not consider a cutoff in our calculations, but this does not affect our validation exercise.

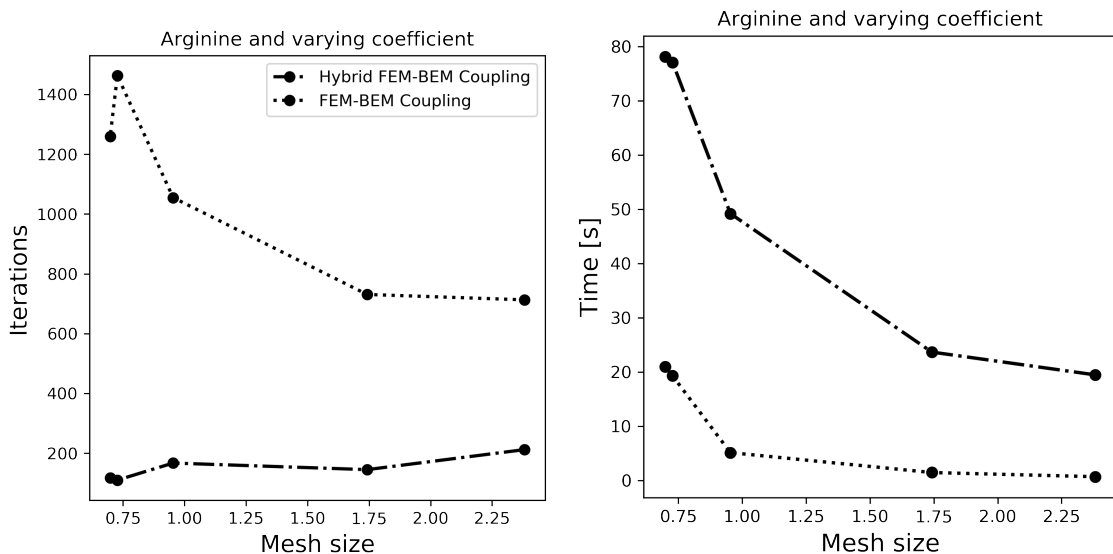


Figure 4: Time-to-solution and iteration count to compute the solvation energy of arginine with a variable permittivity, using standard and hybrid FEM-BEM coupling.

## Convergence and performance for arginine

Table 1 shows a comparison of solvation energy computed with APBS and our FEM-BEM coupling approaches. We can see that they are both converging to equivalent values of solvation energy, where the finest meshes agree up to the third significant figure.

Figure 4 contains performance results of this test case, where we distinguish the iteration count from the calculation in dissolved and vacuum states. Similar to the case with constant permittivity, although the hybrid approach requires less iterations (are we counting them appropriately? meaning there are external and internal iterations), the total time to solution is less for the standard approach. This means that each iteration of hybrid FEM-BEM is slower than the standard counterpart.

## Performance analysis for larger structures

So far, in all the small structures that we have tested, the standard approach has been more efficient than the hybrid one. However, the fact that there are better preconditioning strategies for the hybrid approach indicates that it may become faster for larger test cases, where conditioning of the linear system is usually more important. In this section, we

	Mesh size $\text{\AA}$	$\Delta G_{solv}$ kcal/mol
APBS	$0.39 \times 0.39 \times 0.39$	-32.4042
	$0.26 \times 0.26 \times 0.26$	-32.3375
	$0.17 \times 0.17 \times 0.17$	-32.3413
	Mesh dens. vert/ $\text{\AA}^2$	
Standard FEM-BEM	2	-36.239
	4	-33.129
	8	-32.674
	12	-32.648
	16	-32.293
Hybrid FEM-BEM	2	-35.333
	4	-33.079
	8	-32.660
	12	-32.587
	16	-32.359

Table 1: Solvation energy of arginine with a Gaussian-like permittivity, computed using the standard and hybrid FEM-BEM approaches, and APBS.

compare both approaches for larger structures.

## **First-order heading**

## **Second-order heading**

## **Third-order heading**

## **Fourth-order heading**

# **DISCUSSION**

# **CONCLUSIONS**

# **ACKNOWLEDGMENTS**

## References

1. Coulson, C. A., Rev. Mod. Phys., **1960**, 32,170-177.
2. Malrieu, J.-P., J. Mol. Struct., **1998**, 424, 1-2,83-91.
3. Shaik, S., New. J. Chem., **2007**, 31,2015-2028.
4. Hoffman, R., Schleyer, P. v. R., Schaefer III, H. F., **2008**, 47, 7164-7167.
5. Perdew, J. P., Ruzsinszky, A., Constantin, L., Sun, J., Csonka, G., J. Chem. Theory Comput., **2009**, 5, 902-908.
6. Koros, W. J.; Chern, R. T. In Handbook of Separation Process Technology; Rousseau, E. D.; Russell, B., Eds.; Wiley: New York, **1987**; Vol. 2, Chapter 20, pp 34-45.

Figure 5: Place Figure 1 caption here. In the case of reproduced figures in review articles, you must obtain the publisher's permission and state a suitable notice here along with a citation.

Figure 6: Place Figure 2 caption here. Figures should be uploaded as individual files, preferably .tif or .eps files, at high enough resolution (600 to 1200 dpi) to ensure clarity. Please see the authors guide for more details and specifications. For high quality illustrations, we highly recommend the use of the TikZ package.

Figure 1  
Author A, Author B, Author C,  
Author D  
J. Comput. Chem.

<b>Quantity</b>	<b>Calculated</b>	<b>Observed</b>	<b>Error</b>
Density	5.3	6.3	Within limits
Optical magnification	8.3	90.9	Utterly unacceptable

Table 2: Place table caption here.